The Use of Statistical Image Classification In Assessing Antenna Pattern Measurements

Stuart Gregson, Allen Newell
Nearfield Systems Inc.
19730 Magellan Drive
Torrance, CA, 90502-1104, USA

Christian Feat, Frédéric Viguier
Thales Alenia Space France
26 Avenue Jean François Champollion
BP 33787, 31037 Toulouse, France

***Abstract*— Attempts to produce robust, objective, and quantitative measures of similarity between antenna pattern data sets using statistical methods have been widely reported in the open literature [1, 2]. Hitherto, such techniques have primarily been restricted to the purposes of comparing two or more images as a means in itself. However, no measurement can be considered to be completely free from error, and as such each data set inevitably contains an associated uncertainty. Therefore, in contrast to previous work, this paper discusses and extends some commonly used comparison techniques to take account of the finite, non-zero, measurement uncertainties that complicate the comparison process. Results are presented that illustrate the effectiveness of the comparison method and conclusions drawn.**

I. INTRODUCTION

Comparison techniques essentially involve the extraction of different levels of information that can be defined to exist within measurement data [1, 2]. Thus, measurements can be interpreted as being: nominal, ordinal, interval, or ratio dependant depending on the level of information that is extracted during the measurement process. Defining features from antenna pattern data sets that can then be effectively compared can enable one to establish a measure of their adjacency, *i.e.* similarity. Hitherto, such techniques have primarily been restricted to the purposes of comparing two or more images, *e.g.* comparing far-field two-dimensional radiation pattern of a given antenna having been characterised using two different antenna test facilities. Inevitably, any comparison technique that attempts to confirm the degree of similarity will be complicated by the large quantities of data inherent within the measurement process, the interferometric nature of that data, and the very large measurement dynamic range. However, no measurement can be considered completely free from error, and as such each data set inevitably contains an associated uncertainty. Techniques for establishing measurement uncertainties within near-field measurements are well understood and routinely deployed, *e.g.* the NIST 18 term range assessment (RA) method [3, 4, 5, 6]. In contrast to previous work, this paper discusses and extends some commonly used comparison techniques to take account of the finite, non-zero, measurement uncertainties that are associated with each of the individual measurements. Knowledge of these uncertainties become all the more crucial when measurements are to be compared since the degree of agreement achieved can only be successfully interpreted when this information is taken into account. The method that underpins this comparison therefore utilises results from two RAs, one RA being derived for each of the measurement data sets being compared.

This comparison can be determined by performing repeat measurements where only a single parametric change has been introduced. For the case being considered here, that change corresponded to the substitution of a "model tower" ϕ/θ type spherical near-field (SNF) positioning system with an alternative "overhead scanning arm" θ/ϕ type SNF system. All other parameters remaining fixed. That is to say, the comparison was made using the same: AUT, beam, frequency, SGH, near-field probe, acquisition and processing software, RF subsystem, chamber, tabulating co-ordinate system, polarisation basis, and definition of principal polarisation. The degree of agreement between the two "equivalent" measurements can be assessed qualitatively, through visual inspection, of graphical representations of the measured data using for, example, one dimensional cuts, or two-dimensional false colour checkerboard, *etc.*. Alternatively, quantitative measures of adjacency can be obtained through the extraction of various statistical metrics [1, 2]. Figure 1 and 2 below contain typical false colour checkerboard pattern plots that can be used to qualitatively assess agreement through inspection. Here, the patterns have been resolved onto a circularly polarised Ludwig II azimuth over elevation polarisation basis and have been tabulated using a regular azimuth over elevation co-ordinate system [2]. The same colour axis and contour levels have been used during the preparation of each figure.

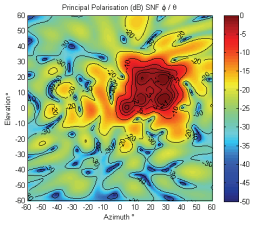

Figure 1. ϕ / θ SNF measurement.

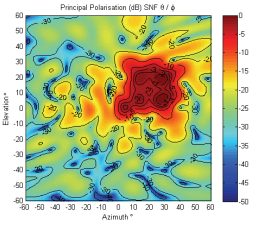

Figure 2. θ / ϕ SNF measurement.

From inspection of the above figures it is clear that the respective principal polarised patterns are in very encouraging agreement. However, without considering the respective uncertainty budgets, it is not possible to say whether these patterns agree to within the experimental bounds. The remainder of this paper is devoted to answering this question commencing with the next section which summarises the signal to stray-signal level concept which, as will be shown, can be used to address this issue.

II. Signal to Stray Signal Level

When evaluating near-field range assessments, the usual method for determining errors through measurement is to isolate and vary a single parameter of the test and observe pattern changes. The change in the measurement parameter is designed to focus on a single error source such as scattering or receiver linearity. Differences in pattern characteristics, *i.e.* gain, side lobe level, cross-pol level, and pointing are then recorded. Often it is possible to describe small pattern differences by computing a signal-to-error level. This signal-to-error ratio can then be used to evaluate the effects of the same error at a different pattern level. Figures 3 and 4 contain a schematic representation of a signal *S* being combined with an error *E*. Here, the true value, designated by *S* is taken to mean the value obtained after an infinite series of measurements have been performed under the same conditions with an instrument not affected by systematic errors [2]. The error is the result of a measurement, *i.e.* the measured value, minus the true value. The measured value is the vector addition of the true value and the error [2]. In practice, the error in a measurement can never be determined it can only be estimated.

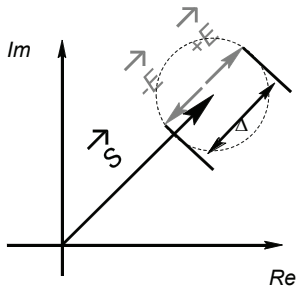

Figure 3. Worst case amplitude error, *S* and *E* in or exactly out of phase.

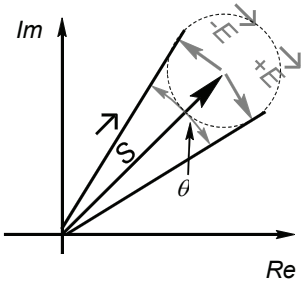

Figure 4. Worst case phase error when *E* and *S* + *E* are in quadrature.

Here, both *E* and *S* are assumed to be complex quantities. The combination of these vectors can be represented through the use of free vectors plotted in the Argand plane with the measured signal being formed from the vector addition using the parallelogram law. The dotted circle represents the locus of possible measured values. Figure 3 shows the case of *S* and *E* being added such that the phases of the error and signal are in phase or exactly 180° out of phase which would result in the largest change in the measured amplitude. From Figure 3 it is clear that the maximum signal is recorded at $S + E$ and the minimum signal is recorded at $S - E$, whereupon the envelope of the measured amplitude value can be expressed as,

$$\text{Measured}\big|_{dB} = 20\log_{10}\left(S \pm E\right) \tag{1}$$

Conversely, Figure 4 contains a combination of *S* and *E* where signals are combined such that the maximum phase change occurs. This happens when the measured signal ($E + S$) is in quadrature with the error signal *E*, with *E* either leading or lagging *S*. Thus, from inspection of Figure 4 it is clear that the maximum phase error can be written as,

$$\theta_{\text{Max}} = \pm\arcsin\left(E/S\right) \tag{2}$$

Usually, we do not know the value of the error as in practice is it the ratio of the signal to the error that is available. Thus, taking equation (1) and expressing it in terms of the signal-to-error ratio *S*/*E* (where S/E is a relative error) we obtain,

$$\text{Measured}\big|_{dB} = 20\log_{10}\left(S \pm \frac{S}{S/E}\right) \tag{3}$$

Factorising this and using the law of logarithms yields,

$$\text{Measured}\big|_{dB} = 20\log_{10}\left(S\right) + 20\log_{10}\left(1 \pm \frac{1}{S/E}\right) \tag{4}$$

Thus, the measured value can be expressed as,

$$\text{Measured}\big|_{dB} = \text{Signal}\big|_{dB} + \text{Uncertainty}\big|_{dB} \tag{5}$$

Here, the term uncertainty is used to mean an estimate or approximation of the error [2]. Thus when assuming the *S*/*E* ratio is expressed in logarithmic form, which it usually is, we can write the upper and lower bound uncertainties as,

$$\text{Upper Bound Uncertainty}\big|_{dB} = 20\log_{10}\left(1 + 10^{-\frac{S/E\big|_{dB}}{20}}\right) \tag{6}$$

$$\text{Lower Bound Uncertainty}\big|_{dB} = 20\log_{10}\left(1 - 10^{-\frac{S/E\big|_{dB}}{20}}\right) \tag{7}$$

Figure 5 contains a plot of the upper bound uncertainty plotted as a function of the signal-to-error ratio whereas Figure 6 contains a plot of the phase error when plotted as a function of the signal-to-error ratio thereby illustrating their respective relationships. By comparing these plots, it is clear that a maximum phase error of 10º or a maximum amplitude error of 1 dB could be produced by the same error level. When taking measurements this is an approximate relationship, *i.e.* rule of thumb, which is often observed.

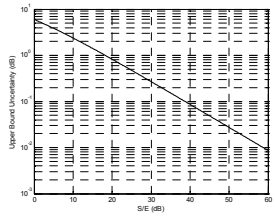

Figure 5. Amplitude measurement error due to signal-to-error ratio.

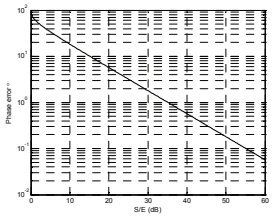

Figure 6. Phase measurement error due to signal-to-error ratio.

Figure 7 illustrates the conversion between S/E and upper and lower bound uncertainties using equations (6) and (7) respectively. When the S/E is high, *i.e.* greater than 25 dB, the difference between the lower and upper bounds is negligible. As the S/E reduces, the difference becomes more pronounced. The measurement uncertainty means that the true value falls somewhere between the upper and lower bounds plus the measurement value. Even though the AUT may not actually have a side-lobe, or cross-polar, value at a particular level, the error can still be evaluated at that level. To illustrate this procedure, consider a side-lobe measured at -45 dB with a 10 dB S/E ratio. From equations (6) and (7) we can see that this will have a true value that lies between the lower bound of -48.3 dB (-45 + -3.3) and the upper bound of -42.6 dB (-45 + 2.4). Thus, for a fixed error level, as the signal level increases, the uncertainty bounds correspondingly decrease. This can be seen illustrated further in Figure 8 which contains a graphical representation of the side lobe level upper and lower bounds as a function of signal level for a fixed error level of -55 dB showing the effect that this has on a side-lobe at varying levels *S*.

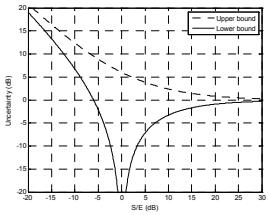

Figure 7. Upper and lower bound amplitude uncertainty plotted as a function of *S*/*E* level.

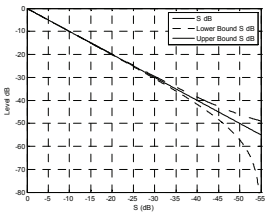

Figure 8. Amplitude Uncertainty plotted at varying SLL for a fixed error level of -55 dB.

Since there is often a "not-to-exceed" specification on sidelobes or cross-pol performance, the upper bound value is usually chosen when the *S*/*E* is low. Since the lower bound can approach -∞, choosing the Upper-bound uncertainty makes sure that the highest level the true value can be compared to is the "not-to-exceed" specification. Although it is strictly mathematically erroneous to do so, for the sake of simplicity, although perhaps at the expense of clarity, many workers state only the upper bound value and ignore the asymmetric nature of the upper and lower bounds. In this way, and as will be shown below, once the measurement uncertainty is known from completing an 18 term range assessment, and by using the antenna pattern function, it is possible to plot the measurement uncertainty in the form of a pattern cut, *etc.*, with an example plot being illustrated in Figure 9.

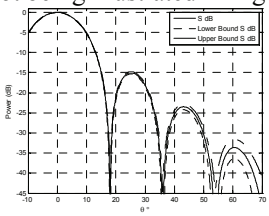

Figure 9. Example of a pattern cut showing upper and lower bounds uncertainties.

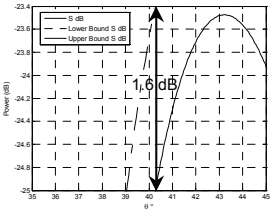

Figure 10. Close up of pattern cut and upper bound uncertainty showing the -25 dB pattern level.

In this way, the upper and lower uncertainty levels can be used to enable "error bars" to be plotted with the antenna pattern. Here, the actual lower bound was used as opposed to choosing the lower bound to be the negative of the upper bound. Conversely, by manipulation of equations (6) and (7), it can be shown that the *S*/*E* ratio can be obtained from the upper and lower bound uncertainties using,

$$S/E\big|_{dB} = -20\log_{10}\left(10^{\frac{\text{Upper Bound Uncertainty}\big|_{dB}}{20}} - 1\right) \qquad (8)$$

$$S/E\big|_{dB} = -20\log_{10}\left(1 - 10^{\frac{\text{Lower Bound Uncertainty}\big|_{dB}}{20}}\right) \qquad (9)$$

Some workers prefer instead to use the inverse ratio, error to signal, *i.e. E*/*S*, in which case the values would be negative which follows from the law of logarithms. In this case equations (6) and (7) can be expressed respectively as,

$$\text{Upper Bound Uncertainty}\big|_{dB} = 20\log_{10}\left(1 + 10^{\frac{E/S\big|_{dB}}{20}}\right) \qquad (10)$$

$$\text{Lower Bound Uncertainty}\big|_{dB} = 20\log_{10}\left(1 - 10^{\frac{E/S\big|_{dB}}{20}}\right) \qquad (11)$$

Similarly, equations (8) and (9) can be expressed as,

$$E/S\big|_{dB} = 20\log_{10}\left(10^{\frac{\text{Upper Bound Uncertainty}\big|_{dB}}{20}} - 1\right) \qquad (12)$$

$$E/S\big|_{dB} = 20\log_{10}\left(1 - 10^{\frac{\text{Lower Bound Uncertainty}\big|_{dB}}{20}}\right) \qquad (13)$$

This provides the expressions in the form that will be used within sections III and IV below. By way of further illustration of the use of equations (10) and (12) in the translation of uncertainties in the context of pattern comparison, let us consider the upper uncertainty at the -25 dB SLL. Using equation (12) we can show that, an upper bound uncertainty of, say, 0.0983 dB at 0 dB equates to an Err/Sig level of -38.876 dB relative to a 0 dB side-lobe. Clearly, relative to a -25 dB side-lobe, this equates to an Err/Sig level of -13.876 dB. Using equation (10) we can see that this corresponds to a 1.601 dB uncertainty at the -25 dB SLL. Figure 10 above contains a variation of Figure 9 only here an Err/0dB Sig level of -38.876 dB has been used and the axes have been adjusted so that the -25 dB antenna pattern level (solid trace) can be clearly seen (centred about the 40° angle). The y-axis of the plot has been chosen to span a scale of 1.6 dB in amplitude. As at the -25 dB pattern level the upper level (dashed trace) uncertainty should be *circa* 1.6 dB above the pattern level and this can be seen in the plot. The following section illustrates how these concepts can be utilised to aid in the measurement comparison process.

III. One-Dimensional Pattern Comparison

The above visualisation strategy illustrates how measurement uncertainties can be incorporated into logarithmic antenna pattern plots. When comparing measurements taken using separate antenna test ranges, it is clear that each individual measurement has an uncertainty associated with it, and that those uncertainties must be considered when comparing the respective antenna patterns. When combining the 18 individual terms within the range assessment, a total value is obtained by taking the RSS of the individual terms. This is valid as each of the terms are assumed to be independent, *i.e.* orthogonal, from one-another. Thus, as each of the antenna pattern measurements that are to be compared can also be considered to be independent, it is possible to combine the respective uncertainties again using a RSS. This enables a total uncertainty to be determined that can be used when comparing one measurement to the other. This one-dimensional measurement comparison can be seen illustrated in Figure 11 and 12 for the L-band principal and cross-polarised pattern measurements respectively. A 130° inter-cardinal cut was chosen for the sake of generality however a similar degree of agreement was attained across all other cuts.

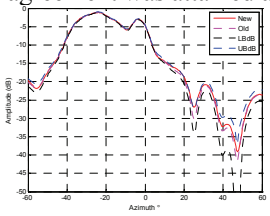

Figure 11. Comparison of principal-polarisation showing uncertainties.

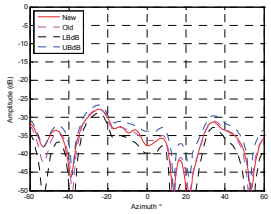

Figure 12. Comparison of cross-polarisation showing uncertainties.

Here, a red trace is used to denote the results from the second measurement (θ/ϕ system) and a magenta dotted trace is used to denote the first measurement (ϕ/θ system). The respective curves are very similar, and difficult to see in the plot, thereby underlining the very high degree of agreement attained. The upper and lower uncertainties are obtained from the combined range assessments are plotted as blue and black dotted traces respectively with the first measurement being used to compute these upper and lower uncertainties. As the upper and lower uncertainties are computed from the first measurement and since those uncertainties contain the combination of uncertainties from both the first and second measurements, then it is possible to say that the measurements agree to within the experimental uncertainties when the second (red trace) falls within these uncertainty levels. That is to say, if the red trace falls between the black and blue traces, the two measurements agree to within the experimental uncertainties. From inspection of the co-polar and cross-polar plots, it is clear that the results agree well and that for almost every angle of interest this condition was satisfied.

Providing each cut contains a large number of data points, a quantitative assessment of the degree of agreement can be obtained by calculating the percentage of points on the second measurement trace that lie between the upper and lower uncertainty traces. As a further measure, this statistic was computed for 19 individual pattern cuts with the mean average of these percentages showing that 95.3% of the points fell within the upper and lower uncertainty bounds as derived from the respective range assessments. By way of a further illustration of the degree of agreement, the mean average across every point in the far-field pattern within the 60° maximum pattern angle was also calculated. In this way, it was found that 95.4% of the far-field pattern points from the second measurement fell within the upper and lower limits. This is a very encouraging result and implies that the agreement attained between the respective pattern measurements was within two standard deviations. That is to say, the agreement between the pattern measurements was circa $2\sigma \sim 95.5\%$. Similarly, from the cross-polarised case, the mean average of the 19 pattern cuts, 95.4 % of the points fell within the upper and lower uncertainty bounds. Again, the mean average across every point in the far-field pattern within the 60° maximum pattern angle was calculated. In this way, it was found that 94.1% of the far-field pattern points from the second measurement fell within the upper and lower bounds which again mean that the cross-polarised patterns agree to 2σ. Thus, we can state that the first and second measurements are in agreement with one-another to approximately 2 standard deviations where this assessment has been performed at all pattern levels and at all pattern angles out to 60° away from boresight. By assuming that the error on this assessment is randomly distributed, then a measure of the uncertainty on this result can be approximated from taking the square root of the sample size. As such, the associated uncertainty on this assessment can be seen to be approximately 0.45%, which is an encouragingly small quantity thereby confirming that the sample size was sufficiently large to enable meaningful statistical analysis to be performed.

Here, the far-field patterns as determined from the two measurements need to be presented in the same way so that the degree of similarity can be gauged. As it is in general impossible to install an antenna within a given antenna measurement system and to perfectly align its axes to those of the range, a correction for imperfections in the antenna to range alignment must be performed. Techniques for implementing these sorts of vector isometric rotations are well understood and their use has become commonplace with an extensive treatment of the antenna-to-range alignment correction being found in the open literature [2]. Once each measured far-field pattern has been corrected for imperfections in the antenna-to-range alignment the patterns can be compared. The antenna-to-range alignment information that is crucial to the successful application of this correction was obtained from an optical survey of the AUT with the relationship between the antenna and the range being co-ordinate systems being described by a nine element (orthogonal and normalised) direction cosine matrix [2]. In this way, all antenna patterns that are presented within this inter-range comparison can be considered to be presented in a single (fiducial) antenna mechanical co-ordinate system. In each case the AUT was installed within the respective SNF facilities having been as accurately and precisely aligned to the axes of the range and the alignment corrections represent very small, second order, effects. Equivalent statistics for the case where the antenna-to-range alignment correction was not applied were evaluated by way of an illustration of the small impact that this second order correction had on the assessment of these results. In this way it was found that when this correction was not applied, the percentage compliance was only degraded by *circa* 0.2% which was not deemed to be statistically significant.

IV. Two-Dimensional Pattern Comparison

Figures 1 and 2 above present, two-dimensional false colour checkerboard plots of the principal polarised far-field patterns for each of the two measurements. These plots were created with the intent of allowing qualitative assessment of the degree of agreement by inspection. An alternative two-dimensional assessment can be made by plotting the iso-level (*i.e.* contour) plots of the respective patterns. Figure 13 contains a contour plot of the principal polarized far-field pattern of the AUT with the iso levels being plotted at the -1, -2, -3, -5, -10, -20, -30, and -40 dB levels from the peak of the pattern. Red contours are used to denote the first (reference) measurement, with black contours being used to denote data obtained from the second measurement.

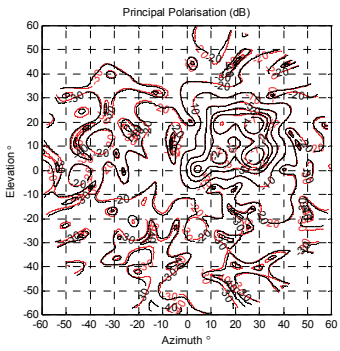

Figure 13. Contour plot comparing principal polarisations.

From inspection of the above figure it is clear that the two measurements are in very encouraging agreement as the displacement between the respective red and black contours is small over the entire 60° forward space. Black contours were plotted on top of the red contours so that when the contours take exactly the same path, the red contours are not visible. This implies that the less red that is visible on this plot; the better the agreement between the respective measurements (if the patterns were in perfect agreement there would be no red contours visible at all). It is important to recognise that this antenna has a very broad main beam pattern as evidenced by the -3 dB contour being circa 30° across in azimuth and elevation at the widest part. This implies that the gain slope of this antenna pattern will be very shallow in this region. As such, any small differences between the patterns will be clearly revealed by differences between the respective contour plots. This observation makes the agreement shown all the more encouraging.

As was the case for the one-dimensional pattern cuts, use can be made of the upper and lower uncertainties in assessing the degree of agreement attained between these patterns. To illustrate this comparison technique, Figure 14 contains an overlay of three contour plots. Here, the red contour denotes the pattern as obtained from the second measurement, whereas the black contour denotes the lower bound uncertainty, and the blue contour denotes the upper bound uncertainties. Please note that for consistency these are the same colours that were used when plotting the one-dimensional pattern cuts as presented above. Here, the second measurement can be said to be in agreement to within the measurement uncertainty providing the red contour lies outside the black contour, and inside the blue contour (this is true for the case where the contour circumscribes a local maximum, the converse is true when circumscribing a local minimum). In this first example as the entirety of the red contour satisfied these constraints, then this pattern contour is 100% compliant. In this case the plotted contour is the -20 dB principal polarization contour. However, at any given pattern level, there may be more than a single contour that is needed to represent the measurement and consequently this analysis must be performed for every contour at the chosen level. Furthermore, this analysis can be repeated at many different levels, and also on the cross-polarized pattern. Figure 14 contains a -33 dB contour of the cross-polarized pattern. Here, whilst for the majority of the length of the red pattern contour it falls outside of the black lower bound uncertainty and inside of the blue upper bound uncertainty, there is a small portion of the length of the contour that violates this condition. Thus, as a small portion of the length of the red contour falls outside of the blue upper bound uncertainty contour and this must be accounted for in the statistics.

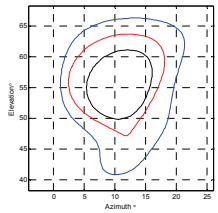

Figure 14. -20 dB contour showing 100% compliance.

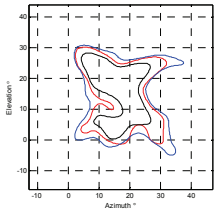

Figure 15. -33 dB contour showing 97% compliance.

As set out above, the red pattern contour is divided into the hundreds of individual line segments that comprise it and a percentage of points that satisfy this constraint can be evaluated. In this case, 96.97% of the line segments satisfy this requirement with a little over 3% of the segments violating this condition. In this way, this analysis can be repeated across the far-field patterns, on both orthogonal polarizations, and over the dynamic range of interest. The use of an iso-level plot means that the comparison is in effect being conducted at a particular level, *e.g.* -33 dB in this case, irrespective of the pattern angle that corresponds to that level. Previously, the comparison was performed as a function of angle for whatever pattern level that angle corresponded to. In this way, the cut comparison and iso-level comparisons can be seen as examining the same data but from different perspectives. This provides useful additional information regarding the pattern agreement.

Following this procedure, percentage compliance statistics were computed using the -1, -2, -3, -5, -10, -15, and -20 dB levels. In this way, the percentage compliance across all of the contours at each of these levels was found to be 93%. This was then repeated for the cross-polarised pattern using the -33 dB level where the compliance was found to be 98%. The choice of the -33 dB level was made as the cross-polar pattern is essentially flat across the majority of the far-field angular span and this level insured that a large number of contours were available for processing. Since, as was also the case with the principal polarisation plots, at a given pattern level there may be: a single contour, more than a single contour, or no contours at all, depending upon the shape of the pattern.

V. Pattern Pointing Comparison

The task of assessing pattern pointing can become complicated if the antenna in question has a particularly broad beam pattern. For the case of a broad beam, *e.g.* isoflux, antenna, the exact location of the peak in the pattern can be disturbed by low level noise or scattering resulting in recourse to alternative assessments. Here, the antenna was found to have an excessively broad beam pattern as evidenced by the shape and size of the -3 dB contour which in this case was found to span *circa* 34° in azimuth, *circa* 29° in elevation at its widest parts. This has a number of consequences for the evaluation of the beam pointing of an antenna pattern. As the gain slope in the vicinity of the greatest region of field intensities is very shallow, this implies that any small change in the pattern (*e.g.* resulting from random noise, *etc.*) can result in the peak of the pattern appearing to be shifted by a large amount. Thus, denoting the peak of the pattern by the location of the largest element within the respective far-field pattern arrays can be very misleading and as such an alternative technique that is more applicable to excessively broad antenna patterns must be utilised.

By comparing the red and black contours in Figure 13 above, it is clear that they are in very close agreement thereby implying that the respective pattern pointing is also in very good agreement. For this reason, when working with excessively broad-beam antenna patterns, such as these, that exhibit very shallow gain slopes, the direction of the pattern is generally assessed by computing the centre of gravity of a

lamina that is formed from an iso-level. That is to say, an *n* dB centroid is used to compare the electric direction of the antenna patterns. Selecting an iso-level such as this means that the deleterious effects of low level noise on a very flat pattern are mitigated thereby enabling useful comparisons to be made. Thus, the -9 dB centroid was calculated for each of these antenna patterns. The -9 dB contour was chosen as the gain slope in the region of the iso-level was steep, this was a distinct single contour, the system dynamic range was sufficiently large that noise was not limiting (*i.e.* impacting) the shape of this contour, and the contour was sufficiently large as to have enough line segments to enable the calculation of the centre of gravity to be reliable. The difference in azimuth pointing was 0.035° or 0.10% of the 3 dB beam-width, and the difference in elevation pointing was 0.026° or 0.09% of the 3 dB beam-width. Here, the degree of agreement between the respective pattern's pointing as derived from the -9 dB centroid is very encouraging. If the true value is assumed to be half way between these two estimates (which is the assumption that is most often adopted) then the pointing is correct to within ±0.017° in azimuth and ±0.013° in elevation. The very broad beam pattern is clearly illustrated by the very small, *i.e.* much less than 1%, pointing differences when these are expressed as a percentage of the -3 dB beam-widths. Finally, by way of a further illustration of the very small impact that the antenna-to-range alignment had on these results, without alignment correction being applied, the equivalent pointing results were within ±0.025° in azimuth and ±0.004° in elevation. Thus, the antenna-to-range alignment correction did have an impact on these results, albeit a very small one.

VI. Summary And Conclusions

Qualitatively, from inspection, for both principal and cross polarized patterns the degree of agreement was found to be excellent. When the experimental uncertainty was also taken into account, as is the case for the pattern comparison cuts and iso-level contour plots, the level of agreement achieved was also deemed to be excellent. It was found that for principal and cross-polarised patterns the measurements were in agreement to approximately 2 standard deviations (*c.f.* 2σ = 95.5%), where this assessment was taken across all pattern levels, and at all pattern angles out to 60° as measured away from the boresight direction. This is clearly a very encouraging result since, as was explained above, although much of the system was kept unchanged between the two measurements, it is important to note that although each measurement was taken in the same test camber, because different spherical positioning systems were used, the respective range boresight directions were orthogonal to one another. Thus, when the patterns are presented in the antenna co-ordinate system, as is the case here, the effects of range reflections will be seen at different pattern angles. Furthermore, as this comparison was primarily directed towards assessing the inherent differences between the respective measurements, no multipath suppression post processing was employed [7] and the aforementioned agreement was achieved in the presence of range clutter. Thus, the degree of agreement attained will only be improved through the use of range reflection suppression.

The above analysis is very powerful as it inherently takes into account the huge dynamic range that is present within the far-field antenna pattern and enables the comparison assessment to be made across the entire far-field angular range of interest. In addition to ascertaining the degree of agreement between the respective antenna pattern measurements, the relative pattern pointing between the measurements was assessed. Again, qualitatively, from inspection of the comparison pattern cuts and contour level plots, it is clear that the results were in very good agreement. Indeed, had there been any significant systematic (*i.e.* residual) pointing differences between the measurements, the percentage compliance for the contour plots would have been significantly degraded. As these were found to be in almost uniformly excellent agreement thus when taken together with the pointing data this confirms that the pattern alignment was very encouraging.

Regarding the statistical assessment itself, it is important to recognise that the novel comparison method presented here is valid when making pattern comparisons at any level as the method inherently compensates for the huge dynamic range present within the data. It also has the advantage that the data is distilled into a single, quantitate, normalised, commutative, robust, coefficient, which for convenience is expresses in the form of a percentage. In addition to this, various graphical representations of the degree of agreement have also been developed and presented. Crucially, it can be seen that for this example, the, localised, pattern cut statistics were found to be in very good agreement with the non-reductionist metrics. Finally, whilst it is clear that there is no "right" answer to the very general question of how best to compare two patterns, research is on-going to establish which combinations of assessment techniques are best suited to the analysis of antenna patterns.

References

[1] McCormick, S.F. Gregson, C.G. Parini, "Quantitative Measures of Comparison Between Antenna Pattern Data Sets", IEE Proc.-Microw. Antennas Propag., Vol. 152, No 6, December 2005, pp. 539-550.

[2] S.F. Gregson, J. McCormick, C.G. Parini, "Principles of Planar Near-Field Antenna Measurements", The Institution of Engineering and Technology, UK, 2007.

[3] A.C. Newell, "Error Analysis Techniques for Planar Near-field Measurements", IEEE Transactions on Antennas and Propagation, vol. AP-36, pp. 754-768, June 1988.

[4] D.W. Hess, "An Expanded Approach to Spherical Near-Field Uncertainty Analysis", AMTA 24th Annual Meeting & Symposium, Cleveland, OH, Oct. 2002.

[5] G.E. Hindman, A.C. Newell, "Simplified Spherical Near-Field Accuracy Assessment" AMTA Annual Meeting & Symposium, 2006.

[6] P. Pelland, J. Ethier, D. Janse van Rensburg, D. McNamara, L. Shafai, S. Mishra, "Towards Routine Automated Error Assessment in Antenna Spherical Near-Field Measurements", The Fourth European Conference on Antennas and Propagation (EuCAP 2010) 12-16 April 2010.

[7] G.E. Hindman, A.C. Newell, "Reflection Suppression in a large spherical near-field range", AMTA, Newport, RI, October. 2005.